

Optical analysis of coatings including diffractive pigments using a high-resolution gonireflectometer

Jiří Filip , Radomír Vávra, Frank J. Maile

© American Coatings Association 2018

Abstract The aim of this article is to demonstrate a new way of measuring and understanding the appearance of pigment flake orientation and texture in special effect pigments for use in industrial coatings. We have used diffractive pigments and analyzed the relative orientation of the particles in the coating layers by evaluating their behavior in two common industry applications: solventborne and powder coatings. We have measured the interference color by taking readings with a high-resolution gonireflectometer, in order to test the viability of automatic diffractive pigment evaluation. The results were analyzed using both psychophysical (i.e., human) and computational (i.e., mechanical) methods. Our later psychophysical and computational analysis of the visual differences that diffractive pigments present in both solventborne (1) and powder coating (2) systems for in-plane and out-of-plane geometries revealed that solventborne liquid paint systems better preserve the appearance of original diffraction gratings. This is due to enhanced orientation of the anisotropic pigment particles. The powder coating surfaces investigated, on the other hand, preserved higher intensity and thus visibility in randomly oriented solitary flakes, creating a greater sparkle contrast. We confirmed our findings by capturing and visualizing coating appearance by means of a bidirectional texture function. We then compared the diffractive pigment evaluation results with other state-of-the-art measuring device readings. We believe that our work provides valuable information on flake orientation and also compares pigment performance

in a range of industrial coating systems, which may enable industrial companies to improve paint spraying processes.

Keywords Diffractive pigment, Particle orientation, Optical analysis, Gonireflectometer

Introduction

Paints and coatings are used for a variety of industrial products, ranging from automotive production to architectural components such as façades, consumer electronics and everyday objects. These coatings have to do more than just fulfill an identification function or act as a mere protective barrier. Today, they are expected to add visual effects “in which visually perceptible properties such as sheen, angular dependency of the color, structure or texture are present by design in addition to the color itself.”¹ Thus, coatings are finishing processes used to improve the visual and functional quality of a surface.² Those containing special effect pigments³ play an important role as they allow designers to make their product look attractive and stand out from the crowd, thereby increasing its appeal. Special effect pigments provide unique visual effects, derived from their chemical composition and physical characteristics. Particle morphology and size as well as flake orientation play a crucial role in achieving these visual effects in a range of applications (e.g., mass pigmentation in plastics, powder/solvent/waterborne coatings, printing, and cosmetics applications).⁴ Thus, all industries that work with platelet-shaped effect pigments are interested in measuring and understanding flake orientation and are looking for simple, noninvasive techniques. Established methods such as the investigation of coating layer cross sections using light and electron microscopy provide only limited statistical 2D information on flake orientation

J. Filip (✉), R. Vávra
The Czech Academy of Sciences, Institute of Information
Theory and Automation, Praha, Czech Republic
e-mail: filipj@utia.cas.cz

F. J. Maile
Schlenk Metallic Pigments GmbH, Roth-Barnsdorf,
Germany

and require a good deal of time and careful preparation skills. This also applies to so-called noninvasive methods such as nano-CT⁵ and OCT.⁶ Today's range of effect pigments is very broad. A good overview is given in reference (3). In our effort to test the viability of a new automatic computational assessment, we selected so-called diffractive pigments for measurement with a gonireflectometer and for the subsequent optical analysis presented³ as the polychromatic effect of these materials is highly angle-dependent. This is due to the anisotropic properties of the pigment morphology (platelet shape) and to the diffractive element present on the surface of each particle.³ These diffractive optics and the grating equation⁷ allowed us to analyze the relative orientation of the particles in the coating layer by capturing their interference color with the help of a high-resolution gonireflectometer.

In this paper, we systematically evaluated visual differences introduced by different coating systems that contain the same diffractive pigment. To assess their behavior, we combined angularly dependent and texture-based analysis of diffraction effect coatings.

The paper is organized as follows. First, diffractive pigments and the coating systems evaluated are discussed in “Introduction” section. “Existing analysis methods for effect coatings to date” section outlines related research and existing analysis methods for pigment behavior. In “Motivation experiment on the visual appearance of diffractive pigments” section, we describe a brief motivation experiment to assess the difference in appearance of diffractive pigments in two different coating systems. “Development of an automatic method of diffractive pigment” section describes our approach to developing an automatic method of diffractive pigment evaluation using a goniometric measurement device and includes detailed information on the experiments conducted. Psychophysical and computational analysis of the obtained data is shown in “Psychophysical analysis” and “Computational texture data analysis” sections, while “Experiments on pigments of varying concentration” section describes additional visual experiments on pigment samples of varying concentration. “Comparison of proposed method to a state-of-the-art texture measurement device” section compares the proposed approach to a state-of-the-art commercial measurement device widely used in the industry. Finally, “Captured appearance on coated objects” section confirms our conclusions by capturing and visualizing the coatings on an object and “Conclusion” section summarizes the main conclusions of the paper.

The use of diffractive pigments in industry

Effect pigments have been widely used for decorative and functional applications in systems such as paints, plastics, printing inks, and cosmetics for several decades.⁸ Their unique ability to achieve eye-catching optical effects, angle-dependent interference colors,

pearl luster or multiple reflections has made them irreplaceable. The use of effect pigments over solid pigments exhibits a number of advantages, e.g., the wide variety of achievable optical effects, the ease of incorporation in all relevant application systems, and the possibility of giving the coated surface extra optical, design-critical characteristics such as sparkle, gonio-, or polychromaticity. It is helpful for industrial users of the pigment to comprehend how the optical appearance of effect pigments is achieved. Access to an automatic diffractive evaluation of their optical appearance, performance, and the use in different coatings will allow such companies to better understand their behavior in application. As analysis of all families of effect pigments would go beyond the scope of this paper, we have focused on diffractive pigments.

The optical appearance of surfaces including diffractive pigments

The optical appearance of a coated surface dramatically changes when diffractive pigments are used as shown in Fig. 1. It is obvious that the three-dimensional object shape leads to surface areas with different colors which depend on illumination and observation angles.⁹

While angle-dependent color is caused by light interference at thin layers and holds true for the majority of effect pigments commercially available today, interference can be achieved by light diffraction of periodically structured surfaces used in diffractive pigments.

Diffractive effect pigments in paint formulations are in fact tiny flakes with a regular grating superimposed on them. Although the flake orientation can be more or less arbitrary, there is almost always an alignment of the majority of flakes in a dry paint which introduces attractive color ringing effects as shown in Fig. 1. The use of diffractive pigments gives industrial paint applications, in particular powder coatings, a completely novel type of appearance; however, due to the strong directional dependence of these pigments and their orientation, any modification in the coating formulation or application process may have an impact on the final flake alignment and consequently on the final visual appearance of the finished product.

Diffraction is seen when light waves encounter obstacles of dimensions similar to their wavelength. A diffraction grating is regarded as an optical component made by a periodic assembly of reflecting or transmitting obstacles (grooves) separated by a distance comparable to the wavelength of light applied. Diffraction gratings disperse beams of white light into the component wavelengths, producing a spectrum. Different types of diffraction gratings are identified and described in detail in references (10) and (11).

The basic principle is explained using an in-plane geometry as shown in Fig. 2 as an example, where incident light from polar angle α is reflected from a



Fig. 1: Example of diffractive pigments used in coatings to produce a shifting multicolored effect on the object

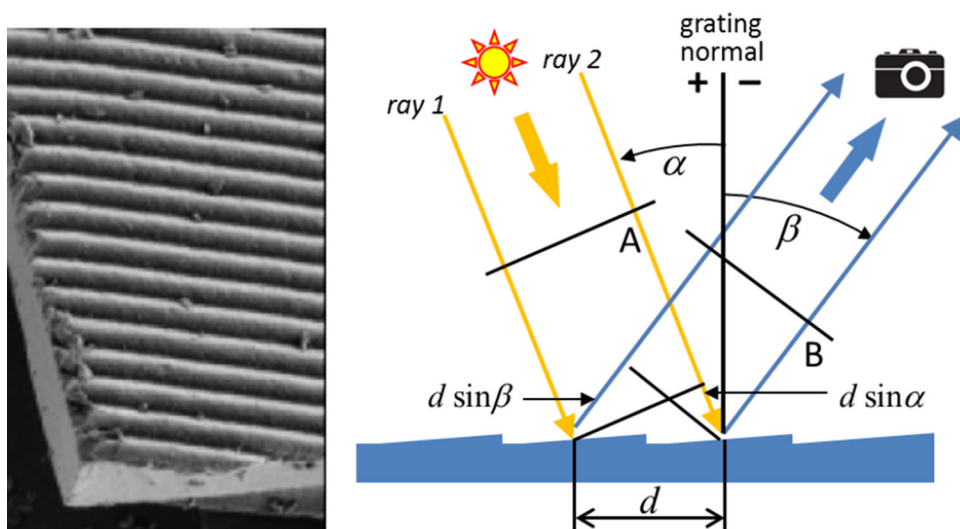


Fig. 2: An close-up view of diffractive pigment (left) and scheme of diffraction for in-plane geometry (right)

grating with a groove spacing d and is observed in polar angle β .⁷

These relations are expressed by the principal grating equation

$$m\lambda = d(\sin \alpha + \sin \beta), \tag{1}$$

where λ is the wavelength of light, and m is the diffraction order, an integer value specifying the order of interest, either negative or positive. The zero order $m = 0$ corresponds to specular reflection. Of course, for out-of-plane geometries, one has to expand this equation using additional azimuthally dependent terms.¹²

The diffraction materials reveal themselves on surfaces as rainbow effects, where each rainbow corresponds to a particular refraction order. Figure 3 depicts the refraction orders on a spherical surface.

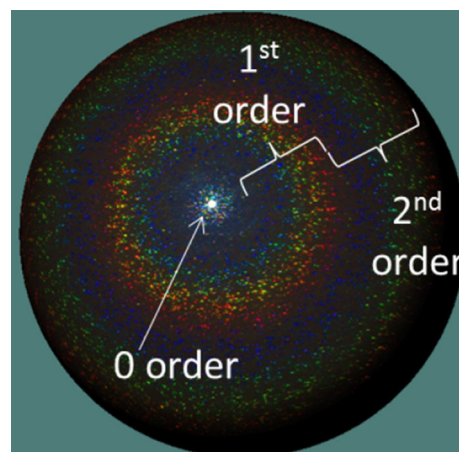


Fig. 3: Refraction orders in diffraction coatings exhibited on a spherical surface illuminated by a point-light as rainbow effects of decreasing intensity

Manufacture of diffractive pigments

The manufacture of diffractive pigments requires a structured polymer film as a template for vacuum deposition of, e.g., aluminum. After metallization, the film is ground into particles and the resulting particles are separated into size fractions. A typical particle thickness is below 1 micrometer, the periodicity of the structure is in the order of 1 micrometer, and its depth is several hundreds of nanometers. Figure 2-left shows a scanning electron micrograph of the structured, diffractive pigment (MultiFlect) discussed in this paper. An important factor for the use of MultiFlect diffractive pigments from Schlenk Metallic Pigments GmbH in our work was the fact that they are supplied in powder form, hence the freedom to use and incorporate them into different paint technologies.

Coating systems analyzed for this study and panel preparation

For this study, the MultiFlect® pigments¹³ were incorporated into two different paint technologies at comparable pigment concentrations:

Paint 1 A liquid, solventborne paint based on polyester/melamine chemistry modified with cellulose aceto-butyrate (CAB). The CAB in the paint formulation improves film shrinkage of the paint layer and is frequently used in effect paints to support pigment particle orientation after spraying the liquid paint onto the substrate.¹⁴ In addition to the CAB, the solvents used in the paint formulation have a significant impact on film formation and shrinkage due to their differing evaporation properties.¹⁵ A detailed discussion of factors influencing effect pigment particle orientation in coatings can be found in reference (4). The liquid paint we used was processed under standard conditions ($T = 21^\circ\text{C}$, 65% relative humidity) in a spray booth using a pneumatic HVLP (high volume low pressure) spray gun¹⁶ and an application robot. The liquid film was sprayed onto steel panels under controlled conditions and dried in a circulating air oven.

Paint 2 A commercially available powder coating based on polyurethane chemistry¹⁷ of 75- μm dry film thickness. Powder technology was used for comparison with solventborne as the literature documents that solvent-free powder coatings exhibit limited effect pigment particle orientation due to different film-forming mechanisms.^{4,14} As the mechanism to improve alignment of the flakes parallel to the polymer surface is absent, light reflection from these randomly oriented pigment particles is lower.

In order to harmonize the physical properties (refractive index, coating layer thickness) of the final layer on the assessed object, both coating types were finished with a commercially available clearcoat based on acrylic chemistry, thus resulting in a 35- μm dry film thickness once the paint had been dried for 15 min at 140°C using a circulating air oven.

Panel preparation We analyzed the (MultiFlect) diffractive pigment¹³ of particle size distribution $D_{50} = 150\ \mu\text{m}$ applied on metal panels painted with a black basecoat. Two different coating technologies were used (as described above): (1) solventborne and (2) powder coating. For one of the experiments an additional method was used: (3) solventborne applied using a doctor blade.

Existing analysis methods for effect coatings to date

Angular analysis of effect pigments in general

A detailed overview of special effect pigments is given in reference (3). Several approaches have been used to analyze angularly dependent bidirectional texture reflectance using flake-based parameters. Kirchner and Cramer¹⁸ analyzed 10 effect pigments of different concentrations using geometries defined by three different instruments. They showed that a specific angularly dependent chroma behavior such as interference and aspecular lines can be used for characterization of specific pigment types. Kirchner and Ferrero¹⁹ illustrated low color variations along isochromatic lines for two Helmholtz-reciprocal in-plane geometries with a series of out-of-plane geometries.

Analysis of coatings containing diffractive pigments

Diffractive pigments are considered as a subset of interference (effect) pigments.²⁰ In contrast to general interference pigments, where the color effects are caused by light waves interference with a substrate coated with materials of high refractive indices, the principle of diffraction is a separation of (disperse) polychromatic light into its constituent monochromatic components. This separation can be achieved by light interference with a diffraction grating of a wavelength close to that of the incoming light.⁷ This produces several diffraction modes that reproduce characteristic rainbow effects whose location depends on a combination of incoming and outgoing directions (see Figs. 1 and 3). One of the first surveys of the application of angle-dependent optical effects deriving from sub-micron structures of films and pigments was presented in reference (21).

Several practitioners and researchers have challenged the difficulty of diffraction pigment characterization using standard industrial spectrophotometers. In reference (22), authors compared the performance of commercial instruments: BYK-mac by Gardner, GCMS-3B by Murakami, and proprietary Gonio-Viewer were used to measure color travel of the polychromatic pigment.²³ Cramer and Maile²⁴ captured and analyzed aspecular behavior of a diffraction

coating in CIE a^*b^* space. They further demonstrated the impact it had when it mixed with an interference effect pigment.

Angularly dependent behavior of diffraction on grating was also a subject of physical and analytical modeling in the past. Rogelj et al.²⁵ calculated bidirectional reflectance distribution functions²⁶ of diffraction gratings for variable grating steps and amplitudes and also studied the relationship between grating parameters and goniophotometric data. Important results were achieved by using electromagnetic and wave optics principles. Such approaches present complex scattering effects resulting from microtopographic surface roughness using Rayleigh–Rice, Beckmann–Kirchhoff, and Harvey–Shack surface scatter theories.²⁷ Recently, Musbach²⁸ applied the theory of field expansion for vector electromagnetic scattering by layered periodic gratings presented in reference (29) to the visualization of polychromatic coatings. Ferrero et al.^{12,30} suggested the analytical expanded grating equation as a geometric term appropriate for intuitive comparison of PCA-based coefficients of various diffraction pigments.²³

Texture analysis of effect coatings

Although these papers demonstrate a gradual expansion of research knowledge on diffractive pigments and its practical applications, the majority of the research was focused on reflectance information only. Aside from diffraction coatings, there are interesting reports on spatial analysis of effect coatings. Kirchner et al.³¹ defined a diffuse coarseness and glint impression under either diffuse or directional lighting as important visual factors. Huang et al.³² proposed a method predicting total visual differences of effect coatings based on variations in color, coarseness, and glint. The method depends on the type of illumination used. Rentschler³³ has shown a systematic variation of sparkle and graininess for different effect pigment types and particle sizes. Ferrero et al.³⁴ proposed to study

contrast and density of sparkle spots at different illumination/observation geometries to establish the sparkle/graininess characteristic of a specific coating. While the contrast is determined by the specular reflectance of the flakes, by their size and by the diffuse reflectance of the coating, the density is determined by the orientation distribution of the flakes and their flatness. Dekker et al.³⁵ psychophysically analyzed color, sparkle, and graininess and used the information to derive a total appearance difference equation. A physical model of sparkling flakes visibility, motivated by astronomical models, was introduced in reference (36). Wang and Luo³⁷ ran several psychophysical studies to validate sparkle and graininess readings of a commercial device BYK-mac. Seubert et al.³⁸ analyzed the relationship between flake orientation and coating appearance and created a model of scattering behavior of metallic paint systems.³⁹

One of the first attempts to capture spatial information of diffraction coatings was published in reference (40). It was shown that the appearance of the diffractive effect pigment used (MultiFlect^{®13} with a median diameter of $D_{50} = 35 \mu\text{m}$) can be effectively captured with the help of the gonioreflectometer in a bidirectional texture function⁴¹ and further for the interactive photorealistic visualization with arbitrary geometry.

Motivation experiment on the visual appearance of diffractive pigments

The following preexperiment was carried out to analyze the differences in appearance between diffractive pigments in a liquid, solventborne system + diffractive pigments, and a powder coating system using the same pigments.

An initial analysis of the panels coated using paint technologies 1 and 2 revealed significant visual differences. For our analysis, we used a byko-spectra effect light booth by BYK-Gardner (see Fig. 4).

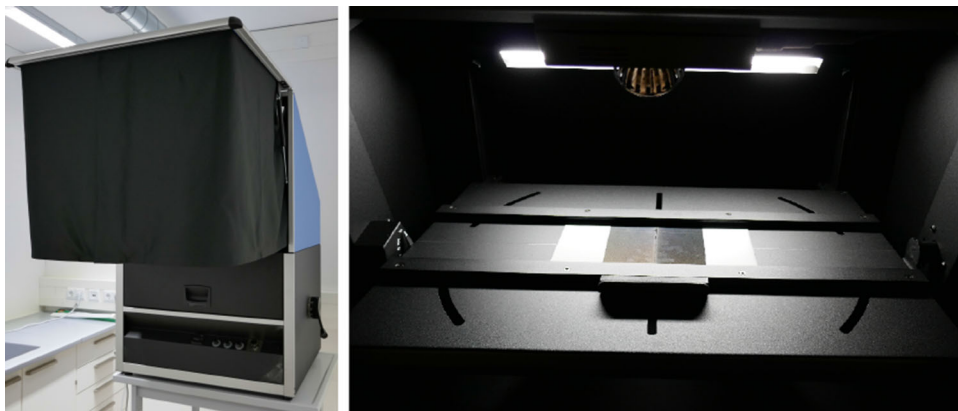


Fig. 4: The byko-spectra *effect* light booth used for our analysis

The booth allows setting of six aspecular observation angles ($-15^\circ / 15^\circ / 25^\circ / 45^\circ / 75^\circ / 110^\circ$) specified in ASTM and DIN standards^{42–44} as shown in Fig. 5. The setting is carried out manually by the observer tilting the holder contacting the sample. The booth has two lighting options (diffuse and directional 45° from a surface normal), and the panels that are to be analyzed are observed through a narrow viewing slit.

A comparison of the behavior of solventborne and powder coatings in the booth for directional illumination is shown in Fig. 6. All images were captured using a Nikon D4 SLR camera. For each geometry setting we compared solventborne and powder-coated panels and the original diffraction foil, which was used as a precursor for the production of the pigment flakes. The powder coating produces more pronounced sparkle, but lacks an overall color-shift effect. On the other hand, the solventborne coating method aligns pigments more uniformly, resulting in an appearance closer to the original diffraction foil.

These marked visual differences were the reason for the development of an automatic method of diffractive pigment evaluation, which is the subject of this paper.

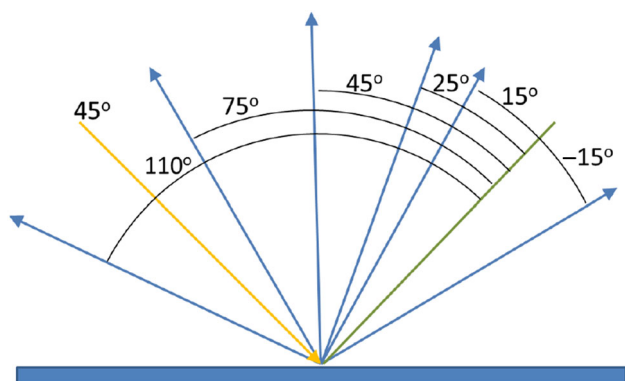


Fig. 5: The viewing geometry for directional illumination 45° from surface normal

Development of an automatic method of diffractive pigment

Appearance acquisition system

We used the gonioreflectometer at UTIA—Institute of Information Theory and Automation,⁴⁵ to capture the appearance of the tested coatings. This state-of-the-art setup (see Fig 7) measures bidirectional reflectance distribution and consists of the measured sample on a rotating stage and two independently controlled arms with a camera (one axis) and a light source (two axes). This allows for flexible and adaptive measurements of nearly any combination of illumination and viewing directions. Although camera view occlusion by the arm with the light source may occur, it can be analytically detected, and in most cases, alternative positioning is possible. The angular accuracy of the light and camera arms positioning is 0.03° across all axes. The inner arm holds the LED light source 1.1 m from the sample and produces a narrow and uniform beam of light. The outer arm holds an industrial, full-frame 16Mpix RGB

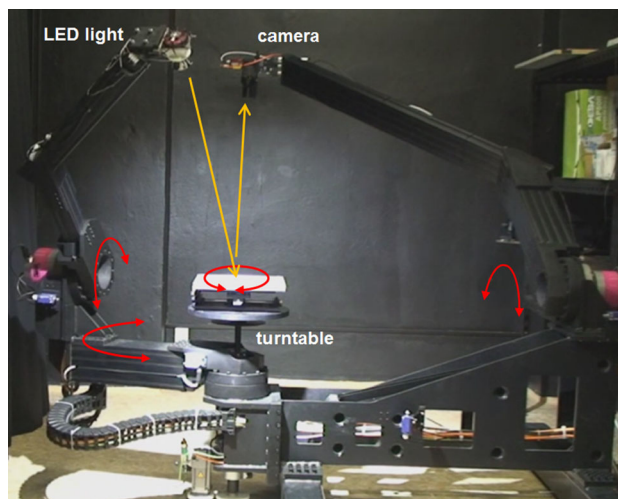


Fig. 7: The UTIA gonioreflectometer

15° aspecular			25° aspecular			45° aspecular			75° aspecular			110° aspecular		
Paint1	Paint2	Foil	Paint1	Paint2	Foil	Paint1	Paint2	Foil	Paint1	Paint2	Foil	Paint1	Paint2	Foil

Fig. 6: Panels sprayed with Paint 1 (solventborne) and Paint 2 (powder coating) incl. diffractive pigment (MultiFlect^{®13} with a median diameter of $D_{50} = 35 \mu\text{m}$) in five geometries of the byko-spectra *effect* light booth compared with an intact structured foil (foil) (employed as a precursor for the manufacture of the diffractive effect pigments used)

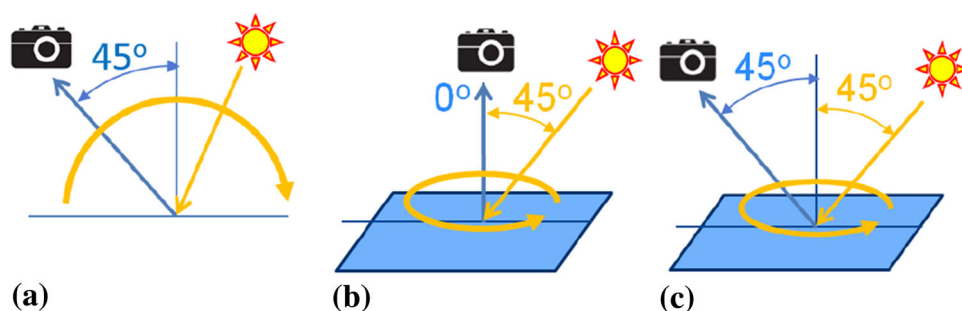


Fig. 8: The illumination/viewing geometry configurations used in our experiments: (a) in-plane, (b, c) out-of-plane

camera (model: AVT Pike 1600C). The sensor's distance from the sample is 2 m. Using different optics, one can achieve a variable spatial resolution of up to 1071 dpi (i.e., $24 \mu\text{m}/\text{pixel}$). In our experiments, we used a resolution of 353 dpi (i.e., $67 \mu\text{m}/\text{pixel}$).

Geometry description

We performed in-plane and out-of-plane analyses. For in-plane analysis, we used the geometry shown in Fig. 8-a, i.e., with the camera fixed at a polar angle 45° from the surface normal, while the illumination polar angles covered the whole plane from -90° to 90° . Note that negative values have the polar angles oriented toward a camera position. Although common multi-angle goniospectrometers⁴⁶ use a reverse in-plane configuration, i.e., fixed light at 45° and variable viewing angles, we resorted to our configuration to avoid perspective and diffractive distortions related to change of viewing angle that would affect the consistency of our image-based analysis. Moreover, from the reflectance point of view, both geometries should produce the same results due to Helmholtz reciprocity.²⁶

In the case of the out-of-plane analysis, we used two geometries. The first had the camera aligned with the surface normal while light circled azimuthally around the material at a polar angle 45° from the surface normal (Fig. 8-b). The second one had the camera fixed at the same polar angle 45° from the surface normal (Fig. 8-c). The sampling step of measurement for all three geometries (one in-plane and two out-of-plane) was one degree. Please note that the in-plane and second out-of-plane geometries have a blind spot of a span of around 25° due to occlusion of the camera's view by the arm with the light.

Figure 9 shows values of individual RGB channels observed for the tested geometries. Included are highlighted approximate angular locations of individual diffraction orders. Note that these effects are completely missing for out-of-plane geometries with a polar viewing angle of 0° .

Analysis

To verify the findings from the goniospectrometer experiment, we carried out a psychophysical and computational (texture data) analysis of two sets of image samples using Paint 1 and Paint 2. In Part 1 we tested whether participants could distinguish between different coating systems (solvent/powder, pigment concentration 1.5%) with the naked eye. Part 2 consisted of the psychophysical validation of the proposed method on dataset (1) solvent/powder, pigment concentration 1.5% for in-plane geometry.

Psychophysical analysis

For the study, we captured data according to the in-plane geometry specified in Fig. 8-a. To make the study tractable, we selected only 17 images at 10° intervals, i.e., angles from surface normal $[-80^\circ \dots +80^\circ]$ corresponding to $[125^\circ \dots -35^\circ]$ aspectual. We showed images of both systems to the subjects side-by-side and in a random order. An example stimulus image is shown in Fig. 10.

A comparison of small portions of images for solventborne (S) and powder coating (P) across the tested geometry is shown in Fig. 11-a. We performed a web-based study online, i.e., under noncontrolled conditions, and split it into two parts. The first and second parts were completed by 81 and 57 subjects, respectively.

In the first part, we tested the subjects' ability to distinguish between the images by asking: *Which of the two images contains more isolated particles?* We used the mean opinion score to obtain results in Fig. 11-b, illustrating that the majority of subjects voted for the solventborne system for all angles, while the closest count of particles was perceived for illumination angles 20° – 40° and 70° – 80° aspectual.

In the second part, we assumed that subjects had already established their visual scales in the first part, and asked them: *Evaluate the visual difference between the images on a scale of 1–5, where 1 means very similar and 5 very different.* The obtained mean opinion scores

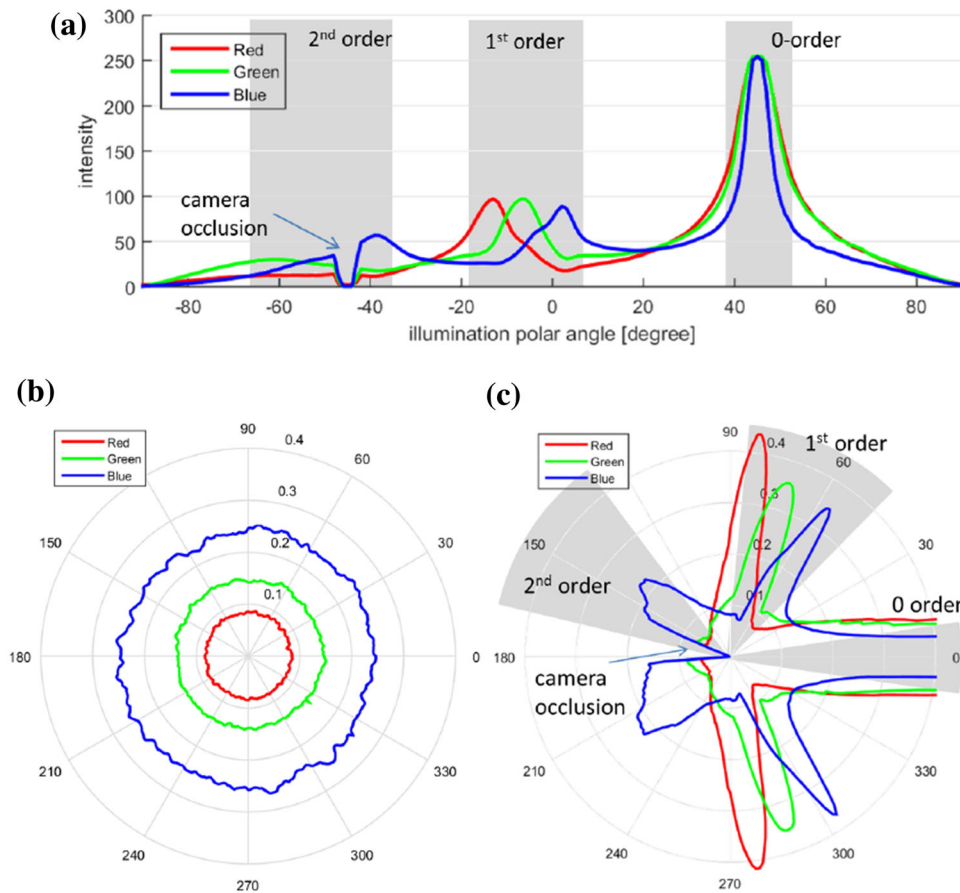


Fig. 9: Distribution refractive orders demonstrated as peaks in average RGB values across (a) in-plane, (b,c) out-of-plane geometries

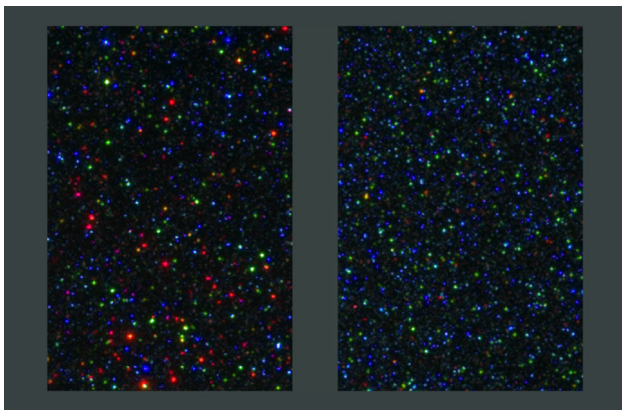


Fig. 10: Example of stimulus image comparing images of coating systems taken at the same geometry

are shown in Fig. 11-c with error bars representing standard deviation across 57 subjects. The graph suggests that subjects consistently perceived relatively high differences for almost all geometries except at extreme lighting polar angles and at angle 75° aspecular.

Finally, we analyzed the reliability of subjects' responses by means of the Krippendorff's alpha⁴⁷ K_α —a statistical measure of the agreement achieved when generalizing several known statistics. The key requirement is agreement observed among independent observers. Output $K_\alpha = 1$ represents an unambiguous indicator of reliability, while 0 does not. K_α values obtained in the experiments were 0.15 and 0.22, respectively. These values express a modest reliability across the subjects, which might be due to the very subjective nature of the subjects' task.

This study proved our assumption that untrained human subjects can distinguish between the solvent and powder-based systems and that the count of particles might be a good candidate for automatic computational analysis which is the subject of the next section.

Computational texture data analysis

The captured in-plane data consisted of 180 RGB images, while the out-of-plane data consisted of 360 RGB images. All images have a high-dynamic range

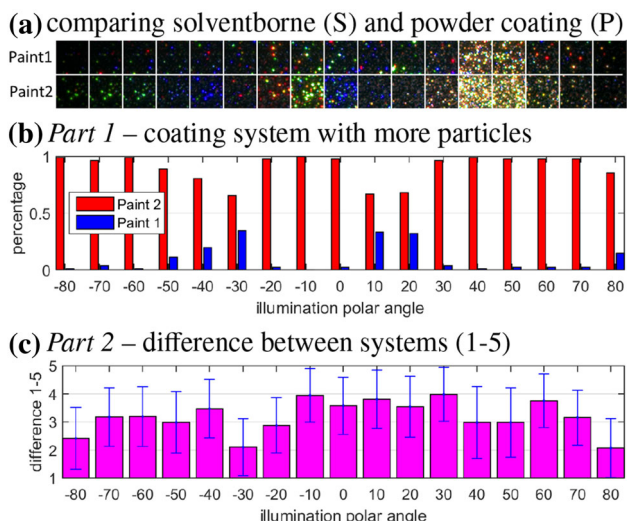


Fig. 11: Psychophysical study: (a) images of the compared samples for all tested geometries, and the results of both parts of the experiment, comparing (b) which of the systems has more isolated particles, and (c) the visual difference between both systems on a scale of 1–5. (a) Comparing solventborne (S) and powder coating (P), (b) Part 1—coating system with more particles, (c) Part 2—difference between systems (1–5).

and spatial resolution of 270×400 pixels corresponding to a sample size of 18×26 mm. To identify the number of visible, i.e., active pigment flakes, we performed the following analysis in each RGB channel. First, we selected a candidate whose image pixels as those had a distinct color in the particular color channel, e.g., for the red channel, the following conditions had to apply

$$(I_R I_G + p_1) \ \& \ (I_R I_B + p_1), \tag{2}$$

where $p_1 = 0.2$, i.e., 20% of the dynamic range of the image and R, G, B denotes individual color channels.

However, these conditions are insufficient in the center of high-reflectance pigments, whose values often tend to be achromatic. Therefore, we extended the color information from the pixel's neighborhood by filtering the image using a Gaussian filter (width 10 pixels, standard deviation $\sigma = 3.0$) to produce a filtered image I^F . The following alternative conditions were used

$$(I_R > p_2) \ \& \ (I_G > p_2) \ \& \ (I_B > p_2) \ \& \ \dots \\ \& \ (I_R^F > I_G^F) \ \& \ (I_R^F > I_B^F), \tag{3}$$

where $p_2 = 0.9$, i.e., 90% of image dynamic range. The equations for the other two channels are similar.

If any of the above conditions for the tested pixel apply, the pixel becomes a candidate for a local sparkle in a respective color channel. To remove visual noise outliers resulting from possible flake interreflections,

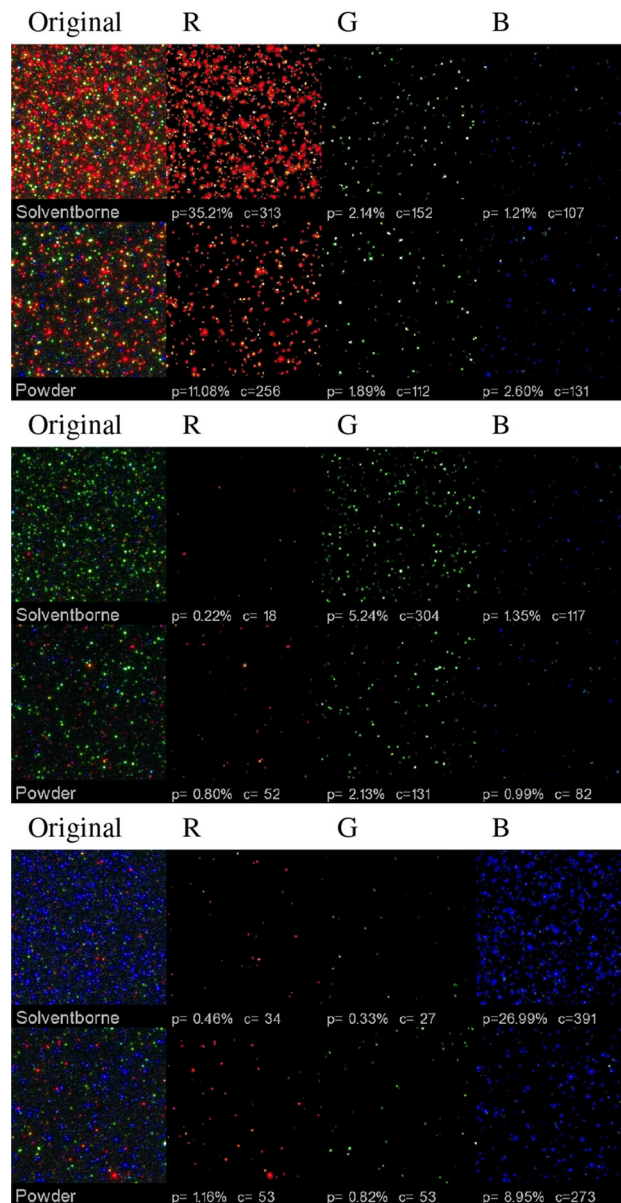


Fig. 12: An example of segmentation of Paint 1 (solventborne) and Paint 2 (powder coating) in isolated pigments in individual color channels. The original image is shown on the left, where p stands for coverage percentage and c for pigment count (Color figure online)

the image is the subject of a morphological opening operator, discarding all elements with a size smaller than 3×3 pixels. Finally, the number of the remaining connected regions and their pixel area is counted. Figure 12 shows examples of identified pigments in each color channel for three illumination directions (with predominantly red, green, and blue pigments). The original image is on the left. The first row shows solventborne, while the second row shows the powder coating.

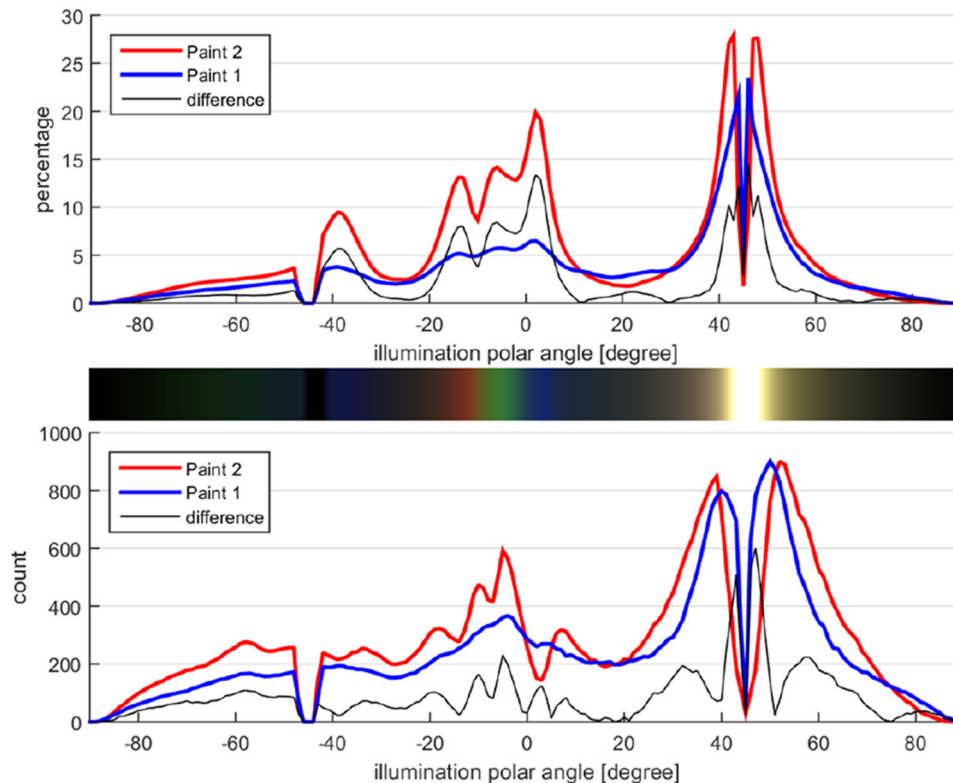


Fig. 13: In-plane comparison of the solventborne and powder coatings in terms of average spatial coverage of visible pigments (top) and number of isolated pigments (bottom) across RGB color channels (Color figure online)

Experiments on pigments of varying concentration

We have tested the proposed pigment characterization method in two independent computational analysis experiments. In the first one, samples of pigmentation 1.5% were used, while in the second one we demonstrated the method's performance on low pigmentations 0.43 and 0.07%, respectively.

In the first step, we analyzed 180 images captured for in-plane geometry (see Fig. 8-a). In addition to the count of effective pigments, we also computed an occupied spatial area (expressed as a percentage of total image area). Figure 13 compares solventborne (red) and powder coating (blue) systems in terms of the percentage of effective pigment's spatial area and pigment count.

In the second step, we analyzed the 360 images captured out-of-plane for both geometries (Figs. 8-b, 8-c). Results again averaged across the RGB channels are summarized in Fig. 14. Apart from a number of effective pigments (a) and their coverage percentage (b), we also evaluated average absolute intensity in effective pigments (c).

Higher pigmentation samples

The results of our analysis of 180 images captured for in-plane geometry are shown in Fig. 13. Please note that the data in the graph relating to the first step of the analysis represent a value averaged across all three RGB channels. The inset bar shows RGB values obtained by averaging original images for different polar angles as shown in Fig. 9-a.

The solventborne coating shows significantly higher values of both observed parameters than the powder coating. Figure 13 also shows the difference between both systems (black outline), which correlates ($r = 0.31$) to the visual difference perceived by human subjects in Fig. 11-c. Note that the lower correlation can be due to the varying sensitivity of human subjects especially near the specular highlight where contrast of individual flakes tends to merge and becomes less apparent.

We then analyzed a further 360 images captured out-of-plane for both geometries (Figs. 8-b, 8-c). Results averaged across the RGB channels are summarized in Fig. 14. Apart from a number of effect pigments (a) and their coverage percentage (b), we also evaluated average absolute intensity in effect pigments (c).

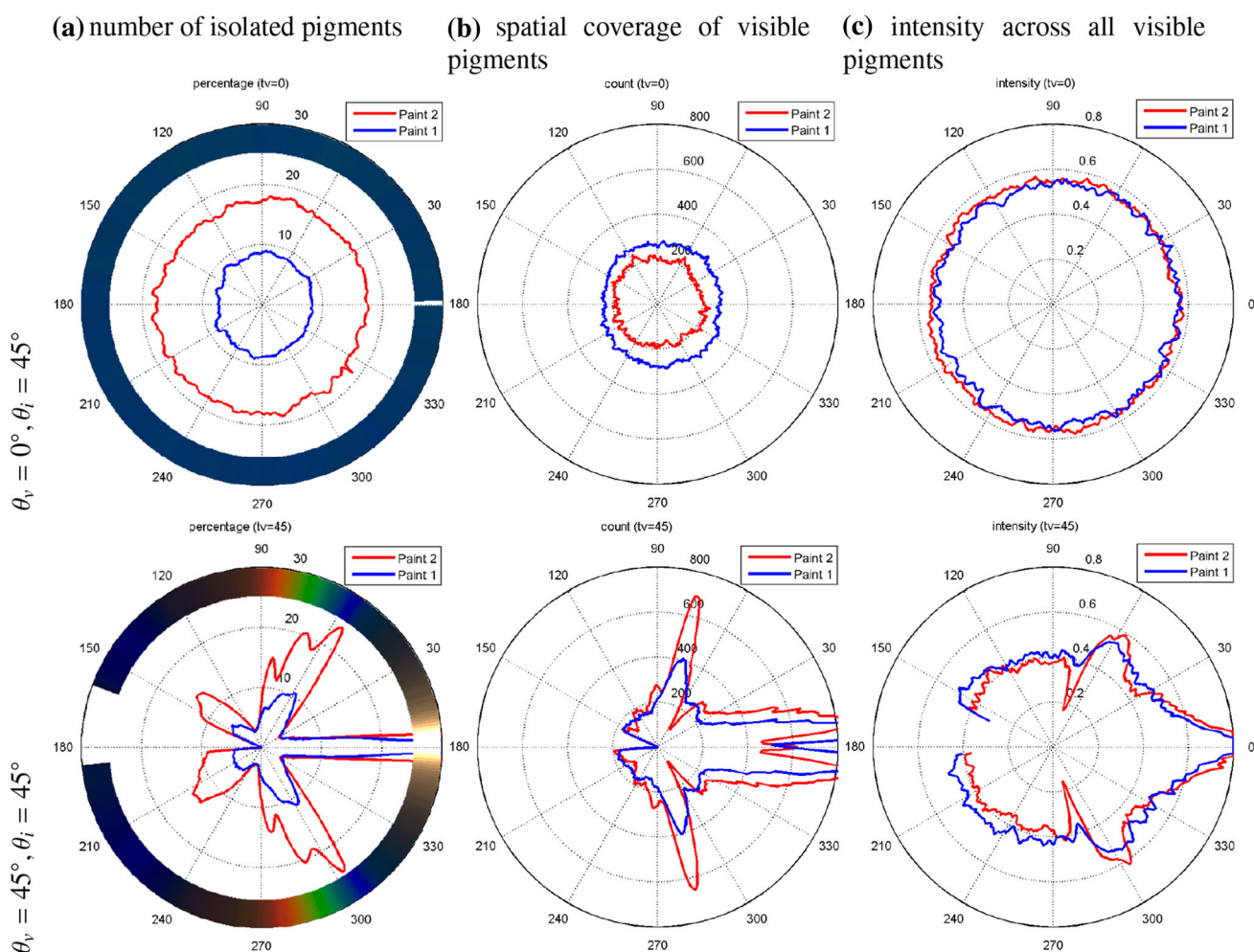


Fig. 14: Out-of-plane comparison of the solventborne and powder coating systems in terms of (a) number of isolated pigments, (b) spatial coverage of visible pigments, and (c) average intensity across all visible pigments across individual RGB color channels. Top geometry $\theta_v = 0^\circ$, $\theta_i = 45^\circ$ Fig. 8-b, bottom geometry $\theta_v = 45^\circ$, $\theta_i = 45^\circ$ Fig. 8-c. The plot in the first row reveals the averaged sample color across azimuthal directions (Color figure online)

In this analysis phase, we observed only a negligible azimuthal dependence for the first geometry shown in the left column (view polar angle $\theta_v = 0^\circ$), and the second geometry shown in the right column (view polar angle $\theta_v = 45^\circ$) exhibits clear azimuthally dependent behavior of all three tested parameters. The most significant differences are again observed near first-order diffraction, especially for the first two parameters: effective pigment count (a) and coverage percentage (b). The biggest differences were found in the blue channel. The values of the solventborne system are almost always higher. The only exception is spatial coverage in the first geometry where the powder-based system prevails. In terms of average pigment intensity (c), the behavior of both systems, is similar, but once we had normalized effective spatial coverage of pigments for both systems we would obtain significantly higher intensity for the powder-based system (especially for the second geometry).

We assume that this is due to the nature of the coating systems: in a solventborne system flakes tend to settle in the solvent, while in powder coating they tend to be fixed close to their initial orientation due to the pigment deposition process. Figure 15 shows an example comparison of flake alignment of both tested coating systems, captured by means of scanning electron microscopy (SEM).

Lower pigmentation samples

This set consists of six samples using diffractive pigments illustrated in Fig. 16. Three of them have a pigment concentration of 0.07% (the first row) and three have a concentration of 0.43% (the second row). The samples in each row differ according to the type of coating system used for identical pigment application. From left to right we used: (1) Paint 2 (powder

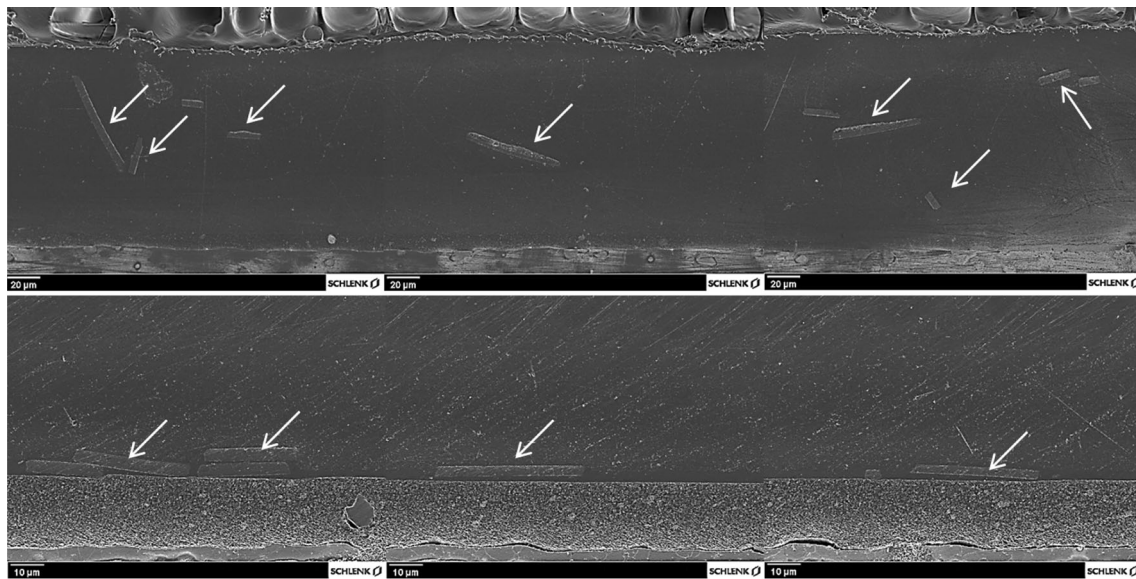


Fig. 15: Investigation of flake orientation for the diffractive pigment particles,¹³ D_{50} value (150 μm) used in Paint 1 (solventborne) and Paint 2 (powder coating) in a cross section using scanning electron microscopy (SEM). Top row: Paint 2 (powder coating) Magnification 500 \times , Bottom row: Paint 1 (solventborne), magnification 1000 \times . The pigment particles in the coating layer of Paint 2 are strongly disoriented in comparison with those of Paint 1

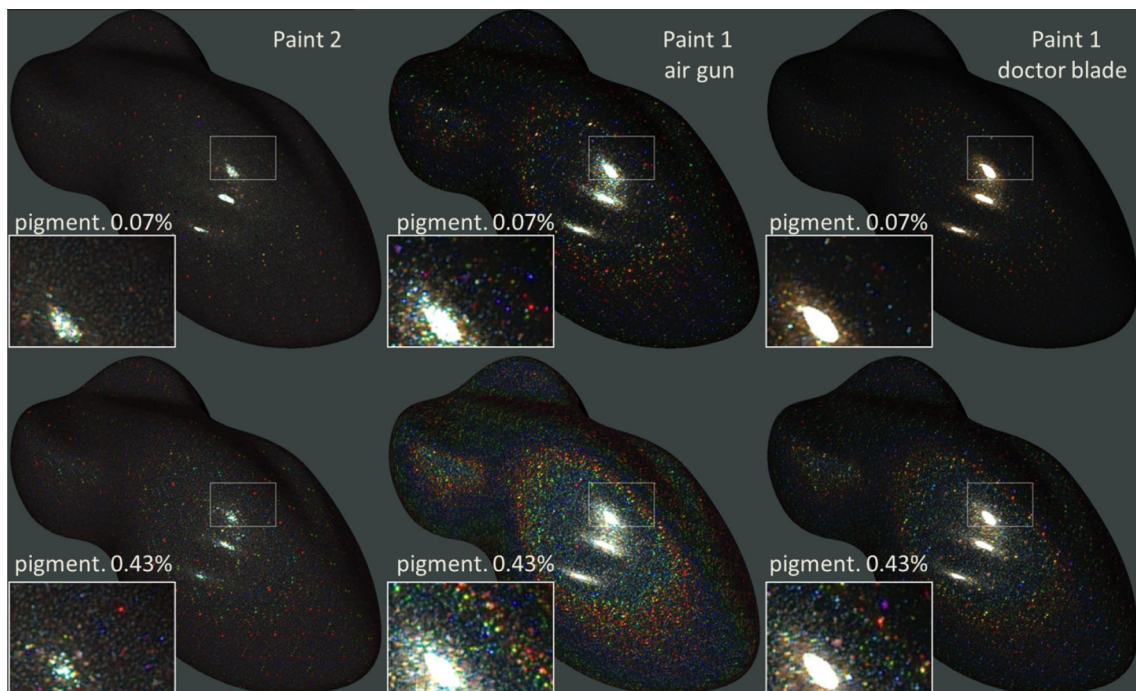


Fig. 16: The sample set of lower pigmentation samples, captured on a flat sample and visualized on a speed shape object, featuring two different pigment concentrations (rows) and three coating systems (columns): (left) Paint 2 (powder coating), (center) Paint 1 (solventborne)—coating film sprayed with air gun, (right) Paint 1 (solventborne)—film generated by coating with a doctor blade

coating), (2) Paint 1 (solventborne)—coating film sprayed with air gun, (3) Paint 1 (solventborne)—film generated by coating with a doctor blade.

After running the same analysis for in-plane geometry, the results are as shown in Fig. 17. The graphs on

the left show results for pigment concentrations of 0.07% and the graphs on the right for concentrations of 0.43%. These graphs suggest that the proposed method can constitute a step toward methods that make it possible to distinguish between coating systems even in

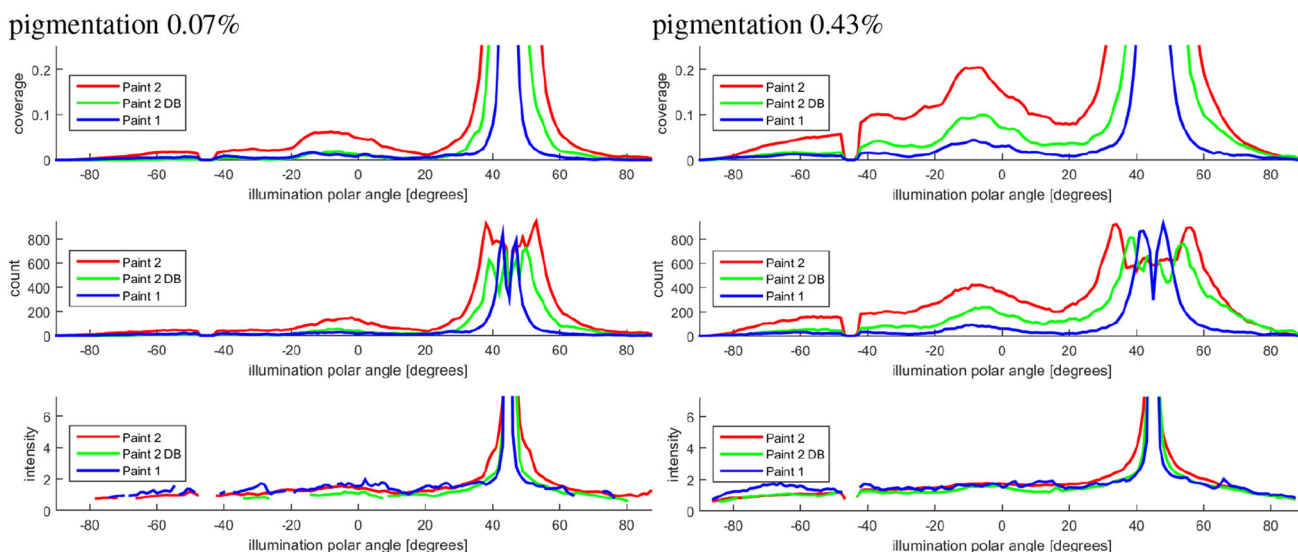


Fig. 17: A comparison of different coating systems within in-plane geometry (red: solventborne, green: powder, blue: the solventborne applied using a doctor blade (DB)) for two pigment concentrations (columns). The first row compares the area coverage by the pigment in %, the second row compares particle counts, and the third row compares average pigment intensity (Color figure online)

very low pigment concentrations. The most obvious difference is for coverage percentage and pigment count.

Comparison of proposed method to a state-of-the-art texture measurement device

We compared our approach to one of the few portable commercial devices that can analyze the texture of special effect coatings, the BYK-mac i.⁴⁸ It captures spectral differences of effect coatings under six aspecular observation angles ($-15^\circ / 15^\circ / 25^\circ / 45^\circ / 75^\circ / 110^\circ$) and illumination 45° from a surface normal, all aligned in in-plane geometry. It also captures the sparkle and graininess textures of the surface (for point-light 45° and diffuse illumination) and computes corresponding readings.

Figure 18 compares sparkle and graininess textures captured by this device for two coating systems (solventborne, powder coating) and two pigment concentrations (0.5 and 1.5%).

While it is hard to tell the difference in the sparkle images using the naked eye, we can observe clear differences in the number of particles for different pigment concentrations in the graininess images. However, there is no obvious difference between the different coating systems.

We also compared the instrument’s proprietary readings of sparkle S_G and graininess G , shown in Table 1. These results also demonstrate that, while the pigment concentration can be differentiated by the proposed measures (as indicated by higher values of graininess for higher concentrations), they cannot

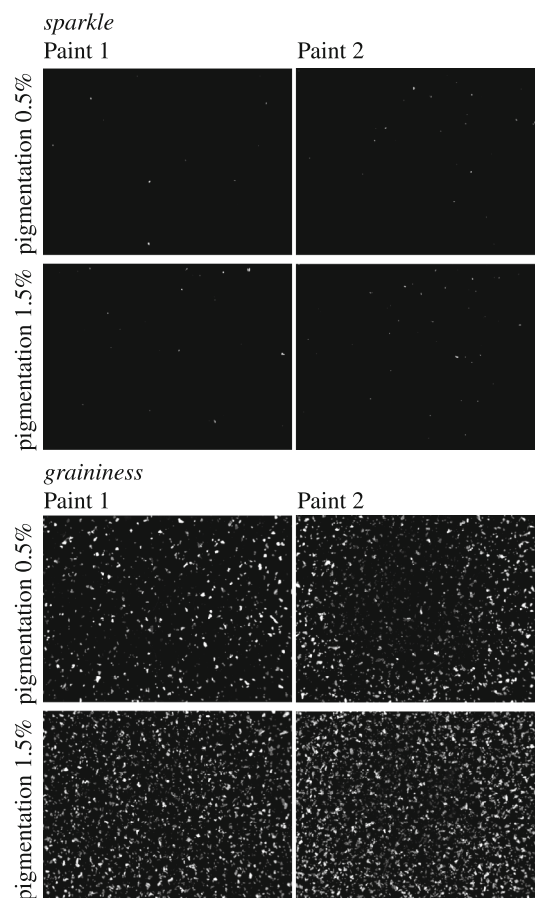


Fig. 18: Texture of coating layers including diffractive pigments generated using a BYK-mac “i” device: left: Paint 2 (powder coating), right: Paint 1 (solventborne)

Table 1: Values of sparkle and graininess as captured by BYK-mac

Sample	Sparkle			Graininess G
	S_G (15°)	S_G (45°)	S_G (75°)	
MF 0.5% Paint 2	10.2	17.3	7.2	12.6
MF 0.5% Paint 1	14.3	15.0	11.2	11.2
MF 1.5% Paint 2	14.1	17.7	21.3	15.9
MF 1.5% Paint 1	18.8	21.2	20.5	15.5

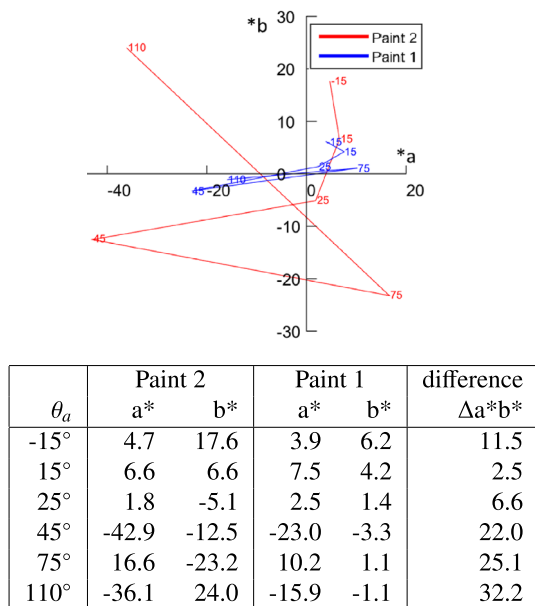


Fig. 19: The CIE a*-b* chart of in-plane geometry for the BYK-mac device side-by-side with original and difference values

consistently distinguish the tested coating systems across different observation angles (due to inconsistent values for sparkle at angles 45° and 75° as highlighted in bold in Table 1).

When we used the device to capture CIE a*-b* charts across in-plane viewing geometry using illuminant CIE-D65 and the CIE-1964 standard observer, we obtained the graph shown in Fig. 19. The figure also includes a table with individual values and chroma differences. Although this chart identifies color differences for different coating systems, the values are too sparse for any meaningful analysis of continuous color travel within the geometry as shown in the further analysis. Possibly, more data can be obtained using the MA98 instrument⁴⁹ designed to characterize complex coatings by capturing additional out-of-plane samples.

In contrast, Fig. 20 demonstrates the CIE a*-b* charts captured for (a) in-plane and (b) out-of-plane geometries using our gonireflectometer. The original RGB values averaged across the entire image were

converted to CIE a*b* using illuminant CIE-D65 and the CIE-1964 standard observer. The graph on the left shows the a*-b* chart for in-plane geometry, where the numbers along the outline correspond to an aspecular angle of light from 110° to -15°. The graph on the right shows an a*-b* chart for the out-of-plane geometry with camera and light fixed at polar 45° and numbers corresponding to the azimuthal angle of light from 0° to 360°. In both graphs, one can observe significantly higher chroma values in the solventborne coating compared to the powder coating across a wide range of colors. Note that the multiangle views and fixed light differ from the BYK-mac instrument, and we can rely on Helmholtz reciprocity²⁶ due to opacity and planarity of the coating samples.

Therefore, to approximate data from the BYK-mac device, we compensated our measurements only for illuminated area foreshortening using a cosine of illumination polar angle. The captured charts describe continuous color travel for both geometries, presenting the central area zoomed on the right side of the chart. Below the zoomed area is a graph demonstrating differences in chroma ($C_{ab}^* = \sqrt{a^{*2} + b^{*2}}$) across all captured geometries, highlighting the angles marking the highest difference between the coating systems. For in-plane geometry such angles are near 43°, 85°, and 50°–60° aspecular. Note that, for out-of-plane geometry, we have two almost overlapping outlines due to azimuthal symmetry of diffractive reflections as shown in Fig. 14. The differences are due to a different distribution of diffractive flakes over a relatively small captured area of 10 × 10 mm.

From these results we conclude that, while BYK-mac i COLOR can, to a certain extent, detect differences between diffractive coating systems based on spectral information, it cannot reliably tell the difference based solely on texture information as was proposed in this paper

Captured appearance on coated objects

To validate the ability of image-based capture and processing methods to distinguish between coating systems used for the application of diffractive effect pigments, we captured the appearance of the tested coatings as a function of the wide range of illumination and viewing directions. Such behavior can be described by a six-dimensional, bidirectional texture function that captures the material surface appearance for incoming and outgoing directions sampled uniformly over hemispheres above the material surface. For the measurement of appearance, we used the gonireflectometer described in “Development of an automatic method of diffractive pigment” section. The hemispheres of incoming/outgoing directions were sampled by means of 81 directions giving a total of 81 × 81 = 6561 images, where each image was taken for a unique bidirectional pair of camera and light positions.⁵⁰ A

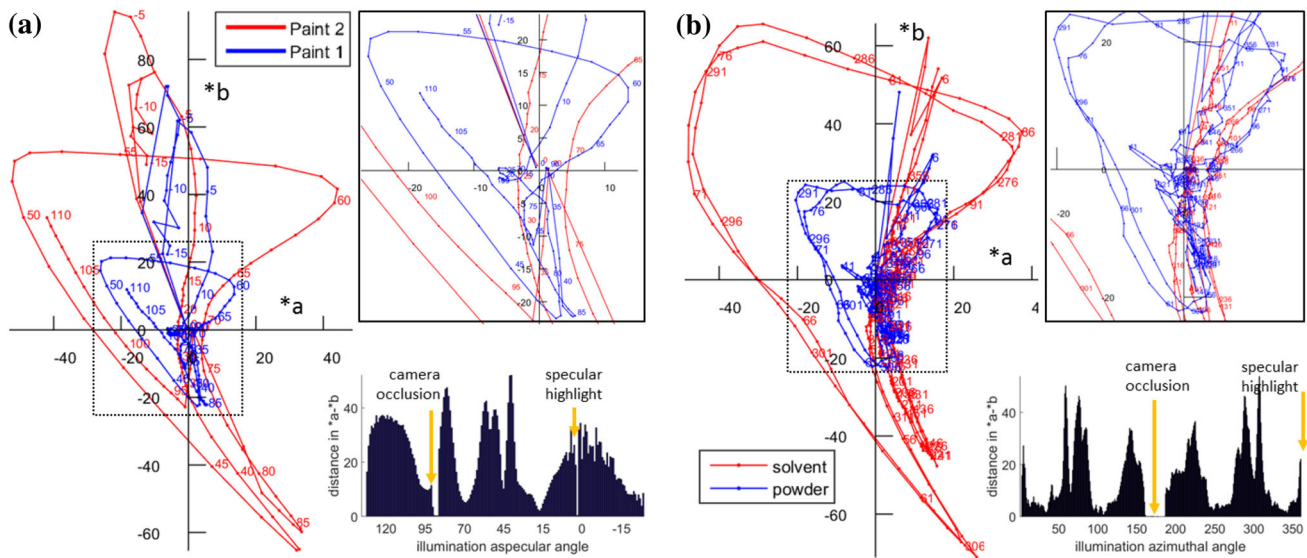


Fig. 20: The CIE a^*-b^* charts of (a) in-plane and (b) out-of-plane analysis comparing solventborne and powder coating systems ($D_{50}=150\ \mu\text{m}$, pigmentation 1.5%) for viewing polar 45° . The right-hand graphs show a zoomed area from the main graphs, and the bottom-right graphs illustrate $\|L\|_2$ differences between the coating systems in a^*-b^* channels across the entire geometry

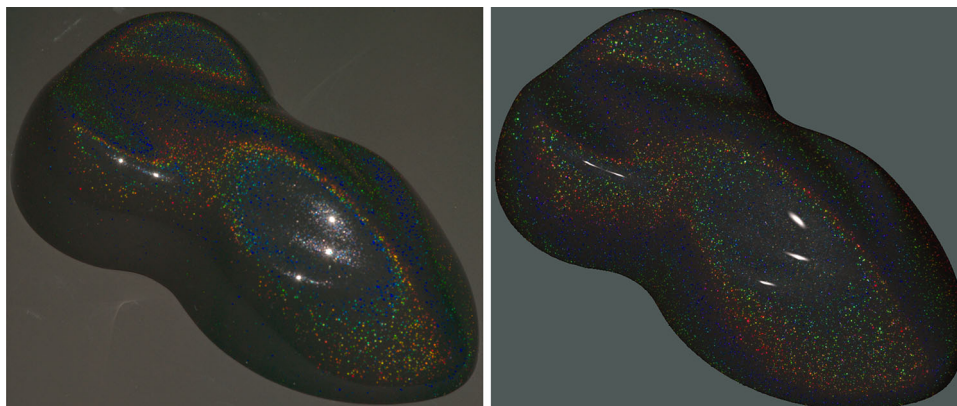


Fig. 21: A comparison of the object photograph (left) to its virtual representation captured by means of bidirectional texture function (right) under point-light illumination (Paint 1 (solventborne)—coating film sprayed with air gun¹³ with D_{50} value $35\ \mu\text{m}$)

small image tile area of approximately 150×150 pixels (corresponding to $10 \times 10\ \text{mm}$) was cropped from the center of each image. The tile is created using a stitching algorithm,⁵¹ guaranteeing seamless edges when the tile is replicated to cover the surface geometry. Therefore, the frontal projection of each pixel covered the spatial area of $67 \times 67\ \mu\text{m}$, while the mean particle size of measured samples was $D_{50}=150\ \mu\text{m}$. Finally, we visualized the captured data on a surface geometry acquired by a laser scan of the real speed shape specimen with a length of 10 cm. The visualization was obtained using an OpenGL Shader. A comparison of the rendered appearance to a photograph of an actual coated object is given in Fig. 21. Note that differences are in the area of specular highlight, due to its undersampling, and due

to light reflections from the table, which are not accounted for in the rendering.

Figure 22 shows a comparison of the solventborne and powder coatings visualized under point-light (the top row) and ambient (the second and third row) illumination. The environment illumination is represented by 144 discrete lights representing the illumination intensity of the actual scene. The material appearance is then shown as a linear combination of individual light contributions. One can observe apparent differences between both systems. While the solventborne coating (on the left) features a more uniform appearance including distinct color ringing effects, the powder coating (on the right) shows more sparkle with overall behavior suppressed. Such behavior agrees well with the results of our pigment behavior

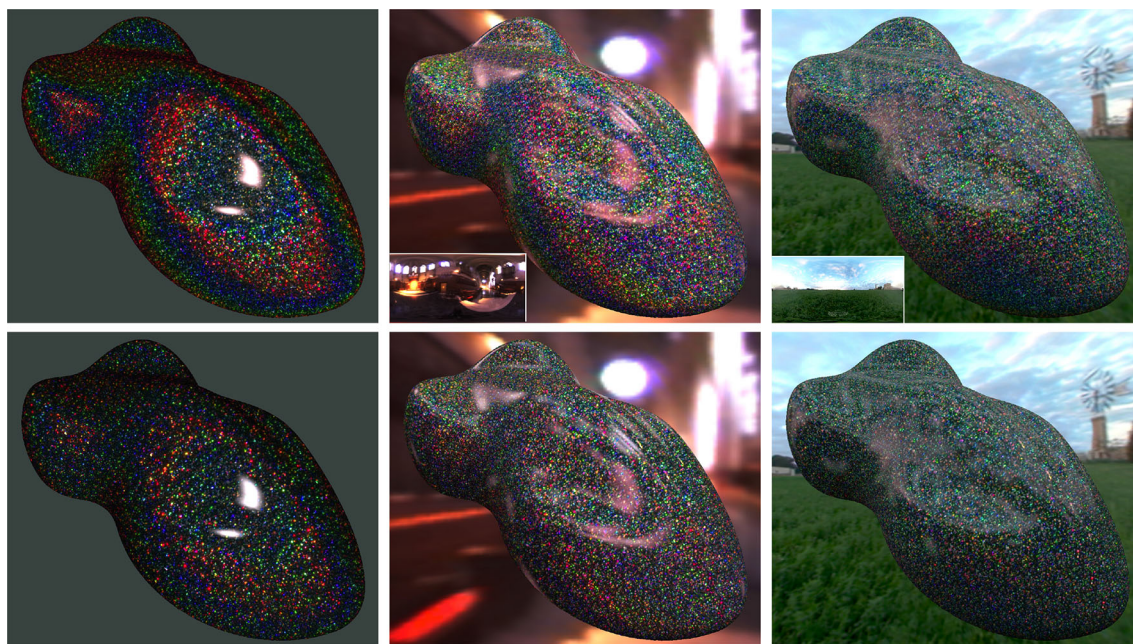


Fig. 22: A comparison of the speed shape coating with Paint 1 (solventborne, top row) and Paint 2 (powder coating, bottom row) under point-light (the first row) and ambient (second and third row) illumination

analysis for in-plane and out-of-plane geometries presented in “[Experiments on pigments of varying concentration](#)” section. Naturally, the more uniform the illumination (going from point-light, indoor to outdoor), the less visually apparent are the differences. This highlights the importance of using a predominantly directional light whenever we need visually to characterize properties of diffractive coatings.

Conclusion

This paper provides a comparative, optical analysis of surfaces modified with two different paint technologies containing diffractive pigments (reference ⁽¹³⁾, $D_{50} = 150 \mu\text{m}$) in one in-plane and two out-of-plane measurement geometries using a gonioreflectometer. Our psychophysical and computational image-based studies in RGB channels revealed that Paint 1 (solventborne) coating achieves significantly better flake alignment as proved by their higher effectively visible numbers and coverage area. On the other hand, the average intensity of pigment flakes is much higher for Paint 2 (powder coating). In summary, we have shown that, in contrast to tested industrial spectrophotometric devices, the data of rather limited spectral resolution, such as RGB triplet captured by our gonioreflectometer, show a promising result that can in the future lead to development of novel differentiation techniques for diffractive coating application systems when comple-

mentary spatial information is taken into account. To accomplish this task one should analyze a substantially larger set of samples including different effect pigments and coating applications.

A flake orientation is influenced by a multitude of parameters within the complete coating manufacturing/spraying process. As effect pigment orientation has a huge impact on the optical appearance of the final coating achieved, the coatings industry is searching for new, cheaper methods which are able to provide information in a noninvasive manner. We believe that our approach is able to provide valuable information on flake orientation of different coating systems, but additionally can be used to compare coating systems and improve paint spraying processes which should be of great industrial importance.

In future work, we plan to combine data from the spatial and angular domain to identify the orientation of individual pigment flakes possibly even in sub-pixel resolution. Another interesting research direction would be the identification of the image statistics applicable for the prediction of pigment-related visual features.

Acknowledgments The authors would like to thank the Schlenk Metallic Pigments team for sample preparation and Dr. Ralf Webler at Schlenk for the SEM analytical support. This research has been supported by the Czech Science Foundation Grant GA17-18407S.

References

- Deutsches Institut für Normung e.V., DIN 55945.
- Becerra, L, *CMF Design-The Fundamental Principles of Colour, Material and Finish Design*. FRAME Publishers, 2016.
- Pfaff, G, *Special Effect Pigments: Technical Basics and Applications*, 2nd ed. Vincentz Network, Hannover, 2008.
- Maile, FJ, Pfaff, G, Reynders, P, “Effect Pigment-Past, Present and Future.” *Prog. Org. Coat.*, **54** (3) 150–163 (2005).
- Rösler, M, Berthold, L, Schischka, J, Heneka, M, “Evaluation of effect pigment orientation using combined SEM, TEM, and X-ray CT analysis and conclusion for interpreting goniospectro-photometric data of effect coatings.” *Asia Color Association Conference*, Rajamangala University of Technology Thanyaburi Faculty of Mass Communication Technology, pp. 180–183, 2013
- Zhang, JB, Williams, M, Lawman, S, Atkinson, D, Zhang, Z, Shen, Y, Zheng, Y, “Non-destructive Analysis of Flake Properties in Automotive Paints with Full-field Optical Coherence Tomography and 3D Segmentation.” *Opt. Express*, **25** (16) 18614–18628 (2017).
- Palmer, C, Loewen, E, *Diffraction Grating Handbook*, Newport Corporation (6th edition), 705 St. Paul Street, Rochester, New York 14605 USA, 2004
- Maile, FJ, Reynders, P, “A Colorful Menagerie of Platelets for Transparent Effect Pigments.” *Asia Pacific Coat. J.*, **23** (1) 14–17 (2010).
- Schmidt, C, Friz, M, *Optical Physics of Synthetic Interference Pigments*, Kontakte pp. 15–15, 1992
- Boyle, E, “Tlmi Seeking Supplier of the Year, Paper.” *Film Foil Convert.*, **78** (4) 36 (2004).
- Fitch, JJ, Fotlano, RA, Josephy, K, Meikka, FN, Meikka, RG, Method of enhancing the visibility of diffraction pattern surface embossment. Eur. Patent No. 0678074B1, 1992
- Ferrero, A, Bernard, B, Campos, J, Perales, E, Velazquez, J, Martinez-Verdu, F, “Multi-angle Colour Characterization of Coatings with Diffraction Pigments.” *Proceedings of the 4th CIE Expert Symposium on Colour and Visual Appearance*, Vol. CIE x043:2016, CIE, pp. 51–59, 2016
- MultiFlect® product information, Schlenk Metallic Pigments GmbH, <http://www.schlenk.com>. Accessed 20 July 2018
- Roberts, AG, Weissberg, SG, “Film-forming Properties of Cellulose Acetate Propionates. Effects of Solvents, Diluents, and Plasticizers.” *Ind. Eng. Chem.*, **43** (9) 2088–2098 (1951). <https://doi.org/10.1021/ie50501a034>
- Mischke, P, *Film Formation in Modern Paint System*, 1st ed. Vincentz Network, Hannover, 2010
- High volume low pressure spraying gun, <https://www.sata.com/index.php?id=hvppistolen&l=1>. Accessed 20 July 2018
- Gillis, P, *Powder Coatings Chemistry and Technology* (2nd edition), Vincentz Network GmbH & Co KG, 2004
- Kirchner, E, Cramer, W, “Making Sense of Measurement Geometries for Multi-Angle Spectrophotometers.” *Color Res. Appl.*, **37** (3) 186–198 (2012).
- Kirchner, E, Ferrero, A, “Isochromatic Lines as Extension of Helmholtz Reciprocity Principle for Effect Paints.” *JOSA A*, **31** (8) 1861–1867 (2014).
- Cramer, W, “Interference Pigments,” *Paint Coat. Ind.*, <http://www.pcimag.com/articles/86923-interference-pigments>. Jan 2007
- Pfaff, G, Reynders, P, “Angle-Dependent Optical Effects Deriving from Submicron Structures of Films and Pigments.” *Chem. Rev.*, **99** (7) 1963–1982 (1999).
- Book, JE, “Measuring Diffractive Color Using Multi-angle Spectrophotometers.” *The Pigment and Colour Science Forum*, 2013
- SpectraFlair® product information, Viavi Solutions, <http://www.viavisolutions.com>. Accessed 20 July 2018
- Cramer, W, Maile, F, “Rainbows Made to Order.” *Eur. Coat. J.*, **4** 52–56 (2016).
- Rogelj, N, Poberaj, I, Gunde, MK, “Goniospectrophotometric Space Curves of Diffraction Gratings and their Applicability as Appearance Fingerprints.” *Appl. Opt.*, **52** (34) 8355–8362 (2013).
- Nicodemus, F, Richmond, J, Hsia, J, Ginsburg, I, Limperis, T, “Geometrical Considerations and Nomenclature for Reflectance.” *NBS Monogr.*, **160** 1–52 (1977).
- Krywonos, A, Harvey, JE, Choi, N, “Linear Systems Formulation of Scattering Theory for Rough Surfaces with Arbitrary Incident and Scattering Angles.” *J. Opt. Soc. Am. A*, **28** (6) 1121–1138 (2011).
- Musbach, A, “Simulation of Paint Films Containing Effect Pigments.” *The Pigment and Colour Science Forum*, 2016
- Nicholls, DP, “Method of Field Expansions for Vector Electromagnetic Scattering by Layered Periodic Crossed Gratings.” *J. Opt. Soc. Am. A*, **32** (5) 701–709 (2015).
- Ferrero, A, Bernad, B, Campos, J, Perales, E, Velázquez, JL, Martínez-Verdú, FM, “Color Characterization of Coatings with Diffraction Pigments.” *JOSA A*, **33** (10) 1978–1988 (2016).
- Kirchner, E, van den Kieboom, G-J, Njo, L, Supèr, R, Gottenbos, R, “Observation of Visual Texture of Metallic and Pearlescent Materials.” *Color Res. Appl.*, **32** (4) 256–266 (2007).
- Huang, Z, Xu, H, Luo, MR, Cui, G, Feng, H, “Assessing Total Differences for Effective Samples Having Variations in Color, Coarseness, and Glint.” *Chin. Opt. Lett.*, **8** (7) 717–720 (2010).
- Rentschler, T, “Measuring Sparkling Blues Without Blues.” *Eur. Coat. J.*, **12** 78–83 (2011).
- Ferrero, A, Campos, J, Rabal, A, Pons, A, “A Single Analytical Model for Sparkle and Graininess Patterns in Texture of Effect Coatings.” *Opt. Express*, **21** (22) 26812–26819 (2013).
- Dekker, N, Kirchner, E, Super, R, van den Kieboom, G, Gottenbos, R, “Total Appearance Differences for Metallic and Pearlescent Materials: Contributions from Color and Texture.” *Color Res. Appl.*, **36** (1) 4–14 (2011).
- Kirchner, E, Van der Lans, I, Perales, E, Martínez-Verdú, F, Campos, J, Ferrero, A, “Visibility of Sparkle in Metallic Paints.” *JOSA A*, **32** (5) 921–927 (2015).
- Wang, ZW, Luo, MR, “Looking into Special Surface Effects: Diffuse Coarseness and Glint Impression.” *Color. Technol.*, **132** (2) 153–161 (2016).
- Seubert, C, Nichols, M, Frey, J, Shtein, M, Thouless, M, “The Characterization and Effects of Microstructure on the Appearance of Platelet-polymer Composite Coatings.” *J. Mater. Sci.*, **51** (5) 2259–2273 (2016).
- Seubert, C, Nichols, M, Kappauf, C, Ellwood, K, Shtein, M, Thouless, M, “A Hybrid Ray-wave Optics Model to Study the Scattering Behavior of Silver Metallic Paint Systems.” *J. Coat. Technol. Res.*, **15** (3) 471–480 (2018).
- Maile, FJ, Filip, J, “New Applications for Polychromatic Effect Pigments.” *Asia Pac. Coat. J.*, **29** (2) 35–38 (2016).
- Dana, K, van Ginneken, B, Nayar, S, Koenderink, J, “Reflectance and Texture of Real-world Surfaces.” *ACM Trans. Graphics*, **18** (1) 1–34 (1999).

42. DIN-6175-2, *Tolerances for Automotive Paint. Part 2: Goniochromatic Paints*, Berlin, Germany: Deutsches Institut für Normung.
43. E2194-12, A, *Standard Practice for Multiangle Color Measurement of Metal Flake Pigmented Materials*, ASTM International, West Conshohocken PA, 2012
44. E2539-12, A, *Standard Practice for Multiangle Color Measurement of Interference Pigments*, ASTM International, West Conshohocken PA, 2012
45. Filip, J, Vávra, R, Haindl, M, Zid, P, Krupicka, M, Havran, V, “BRDF Slices: Accurate Adaptive Anisotropic Appearance Acquisition.” *Proc. 26th IEEE Conference on Computer Vision and Pattern Recognition, CVPR*, pp. 4321–4326, 2013
46. Perales, E, Chorro, E, Viqueira, V, Martínez-Verdú, FM, “Reproducibility Comparison Among Multiangle Spectrophotometers.” *Color Res. Appl.*, **38** (3) 160–167 (2013).
47. Hayes, AF, Krippendorff, K, “Answering the Call for a Standard Reliability Measure for Coding Data.” *Commun. Methods Meas.*, **1** (1) 77–89 (2007).
48. BYK-mac i COLOR product information, BYK-Gardner GmbH, <https://www.byk.com/en/instruments/products>. Accessed 20 July 2018
49. MA98 Multiangle Spectrophotometer Product Information, X-Rite, <https://www.xrite.com/categories/portable-spectrophotometers/ma98>. Accessed 20 July 2018
50. Filip, J, Haindl, M, “Bidirectional Texture Function Modeling: A State of the Art Survey.” *IEEE Trans. Pattern Anal. Mach. Intell.*, **31** (11) 1921–1940 (2009).
51. Somol, P, Haindl, M, “Novel Path Search Algorithm for Image Stitching and Advanced Texture Tiling.” *WSCG*, pp. 155–218, 2005